IEEE Access
Multidisciplinary | Rapid Review | Open Access Journal

Received March 22, 2018, accepted April 27, 2018, date of publication May 7, 2018, date of current version June 5, 2018.

Digital Object Identifier 10.1109/ACCESS.2018.2833858

Robustness Evaluation of Extended and Unscented Kalman Filter for Battery State of Charge Estimation

CHAO HUANG[1,2,3], (Member, IEEE), ZHENHUA WANG[4], ZIHAN ZHAO[5], LONG WANG[6], (Member, IEEE), CHUN SING LAI[1,7], AND DONG WANG[2]

[1]School of Automation, Guangdong University of Technology, Guangzhou 510006, China
[2]Department of Systems Engineering and Engineering Management, City University of Hong Kong, Hong Kong
[3]Guangdong Provincial Key Laboratory of New and Renewable Energy Research and Development, Guangzhou 510640, China
[4]College of Water Resources and Architectural Engineering, Shihezi University, Shihezi 832003, China
[5]School of Geosciences and Surveying Engineering, China University of Mining and Technology-Beijing, Beijing 100083, China
[6]School of Computer and Communication Engineering, University of Science and Technology Beijing, Beijing 100083, China
[7]School of Civil Engineering, University of Leeds, Leeds LS2 9JT, U.K.

Corresponding authors: Zhenhua Wang (wzh2002027@163.com) and Long Wang (long.wang@ieee.org)

This work was supported in part by the Guangdong Provincial Key Laboratory of New and Renewable Research and Development under Grant Y807s61001, in part by the Grant from the Financial and Education Department of Guangdong Province 2016[202]: Key Discipline Construction Programme, in part by the Education Department of Guangdong Province: New and Integrated Energy System Theory and Technology Research Group, in part by the Fundamental Research Funds for the Central Universities under Grant 06500078, and in part by the National Key Research and Development Plan Research and Application of Water and Fertilizer Integration Technology Model for Cash Crops under Grant 2017YFD0201506.

ABSTRACT In this paper, the robustness of model-based state observers including extended Kalman filter (EKF) and unscented Kalman filter (UKF) for state of charge (SOC) estimation of a lithium-ion battery against unknown initial SOC, current noise, and temperature effects is investigated. To more comprehensively evaluate the performance of EKF and UKF, two battery models including the first-order resistor-capacitor equivalent circuit and combined model are considered. A novel method is proposed to identify the parameters of the equivalent circuit model. The performance of SOC estimation is evaluated by employing measurement data from a commercial lithium-ion battery cell. The experiment results show that UKF generally outperforms EKF in terms of estimation accuracy and convergence rate for each battery model. However, the advantages of UKF over EKF with the combined model is not as significant as with the equivalent circuit model. Both EKF and UKF demonstrate strong robustness against current noise. The updates of model parameters corresponding to operational temperatures generally improve the estimation accuracy of EKF and UKF for both models.

INDEX TERMS Extended Kalman filter, lithium-ion battery, robustness, state of charge, unscented Kalman filter.

I. INTRODUCTION

In the auto industry, electric vehicles (EVs) have attracted increasing attention and achieved ever better development as an important technology to reduce the greenhouse gas emission and the consumption of natural resources [1]. Battery system, as one of the key parts in EVs, plays significant role in determining the efficiency, reliability, and safety of EVs systems. Due to the demanding driving operations, a battery management system (BMS) is required to guarantee the good performance of the battery. An accurate estimation of state of charge (SOC) is one of the main functions for a BMS [2], [3]. The SOC quantifies the remaining charge of the battery, which indicates the remaining available range for EVs. Correct SOC estimation can decrease the risk of over-charging/discharging [4], improve the efficiency of the whole EVs energy management, and extend the battery cycle life [5]. Nevertheless, the battery is a strong nonlinear and time-variable system due to its complicated internal electrochemical process, which makes it difficult to directly measure the SOC. Moreover, various factors such as ambient temperature, battery aging, and charging/discharging current rate affect the accuracy of SOC estimation [6], [7]. Thus, a robust

and time-saving technique is required to estimate the SOC on-board.

A variety of approaches have been proposed to estimate the SOC including coulomb-counting methods [8], machine learning methods [9], and state observer methods [10]. Coulomb-counting is widely used in many commercial battery management systems as it is simple and can be easily implemented online. This approach constantly measures current, and simply integrates the charge and discharge current with respect to time, which makes this method highly depend on the precision of current sensor and the accuracy of initial SOC [11]. In [12], an enhanced coulomb-counting method is proposed to improve the SOC estimation efficiency by considering the charging and operating efficiencies. Moreover, coulomb-counting is an open-loop estimator that accumulated error and uncertainties can lower the accuracy of SOC estimation. To reduce initial SOC error and accumulated error, the open-circuit voltage (OCV) method [13], which estimates SOC according to the mapping between OCV and SOC, is employed to recalibrate SOC. Unfortunately, the OCV method requires long-time relaxation to reach steady state, which makes it not suitable for onboard SOC estimation.

For machine learning methods, nonlinear relationship between SOC and relative factors is described by powerful intelligent computational algorithms such as artificial neural networks (ANNs) [14], fuzzy logic [15], and their hybrid approaches [16], [17]. Given an appropriate training data set, machine learning methods can provide good estimation of SOC. In [18], the measured parameters including current, voltage, and temperature are used as inputs of a Gaussian process regression model to predict SOC, and the proposed method outperformed state-of-the-art techniques for SOC estimation. However, it's time consuming to train the model, and the performance of these methods relies on the amount and the reliability of the training data set. Once the operating conditions exceed the training data set, the robustness can be poor, and the uncertainty of the testing data set can exacerbate the prediction error.

Recently, model-based state estimating methods are widely applied into SOC estimation. The accuracy of such methods highly depends on the battery model and the observer. The frequently utilized battery models include physics-based models. References [19], [20], equivalent circuit models [21], [22], machine learning models [23], [24], and empirical models [7]. The design of observers to estimate the state can be in different ways, such as Kalman filter family [25], [26], sliding observer [10], [24], H-infinity observer [27], [28], and Luenberger observer [29], [30]. Among all the kinds of observers, Kalman filter family takes up the largest percentage. Extended Kalman filter (EKF) was introduced to estimate SOC of a lithium-ion polymer battery by Plett [31] in 2004. Later, sigma-point Kalman filter was proposed to improve estimation accuracy [32]. Simultaneously, the methodologies to enhance the Kalman filter family's performance on SOC estimation emerged, such as adaptive extended Kalman filter (AEKF) [33], adaptive unscented Kalman filter (AUKF) [34], square root spherical unscented Kalman filter [35]. In [36], the EKF was applied into SOC estimation and the performance was improved by updating the parameters related to aging. Zou *et al.* [37] developed a deterministic version of EKF for the estimation of SOC and state of health (SOH) in a lithium-ion battery. Meanwhile, studies have been conducted to compare the performance of different state estimating approaches. In [7], the performance of EKF, UKF, and particle filter (PF) were compared in terms of accuracy and computational cost for SOC estimation under various loading profiles, and the experimental results show that the UKF was most robust to unknown initial SOCs.

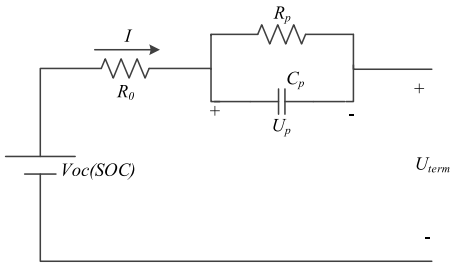

FIGURE 1. Schematic of Lithium-ion battery equivalent circuit.

In this paper, the robustness of EKF and UKF in SOC estimation of lithium-ion battery against unknown initial SOC, current noise, and temperature will be investigated. In SOC estimation, incorrect initialization of SOC is inevitable which is considered as one of the biggest problems of coulomb-counting for SOC estimation. Moreover, the current sensor is much more precise in the laboratory than in the industrial applications which requires robust state observers with strong robustness against current noise. Temperature can significantly affect the performance of lithium-ion battery in discharging capacity, OCV-SOC relationship, and model parameters which can deteriorate the model accuracy. Thereby, the investigation on the robustness of EKF and UKF against those factors is of great value for accurate SOC estimation.

The battery model is essential for SOC estimation using EKF and UKF, therefore two models namely first-order RC (resistor-capacitor) equivalent circuit model and combined model are considered. With first-order RC equivalent circuit model, the recursive least square (RLS) algorithm [36] is frequently applied to identify the model parameters. In this paper, multi-swarm particle swarm optimization (MPSO) [38] will be applied to derive model parameters and compared with RLS algorithm in terms of modeling accuracy.

The remainder of the paper is organized as follows: Section II introduces the battery models, the experiments, and the methods to identify model parameters. In section III, the EKF and UKF algorithms are briefly introduced, and this is followed by experiment results and analysis in SOC estimation. Finally, conclusions of the paper are given in section IV.

FIGURE 2. Schematic of Lithium-ion battery test bench.

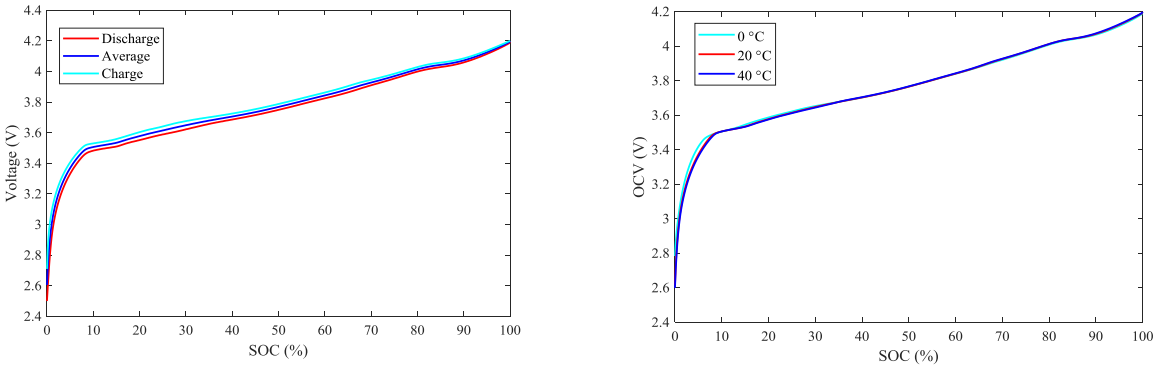

FIGURE 3. OCV-SOC curves: (a) OCV curve at room temperature; (b) OCV curve at 0 °C, 20 °C, and 40 °C.

II. BATTERY MODELING

A. DEFINITION OF SOC

SOC is defined as the ratio of the remaining charge to the maximal capacity of an operating battery [39], and it is computed by

$$SOC_t = SOC_0 - \frac{1}{C_{\max}} \int_0^t i(\tau) d\tau \tag{1}$$

where SOC_t is the SOC at time t, SOC_0 is the initial value of SOC, $i(\tau)$ is the instant loading current assuming positive for discharging and negative for charging, and $C_{\max}$ is the maximal capacity of the battery which can be different from the nominal capacity due to temperature effect and aging effect.

B. MODEL STRUCTURE

In this paper, two models are used to characterize the battery dynamic behavior for EVs' application.

1) EQUIVALENT CIRCUIT MODEL

The first-order RC model shown in Fig. 1 [40] is considered and the electrical characteristic of the model can be discretely expressed as follows:

$$SOC_{k+1} = SOC_k - \frac{\Delta t_k}{C_{\max}} I_k + \omega_{1,k} \tag{2}$$

$$U_{p,k+1} = \exp\left(-\frac{\Delta t_k}{R_p C_p}\right) U_{p,k} + R_p \left(1 - \exp\left(-\frac{\Delta t_k}{R_p C_p}\right)\right) I_k + \omega_{1,k} \tag{3}$$

TABLE 1. Specification about the Test Battery.

Type	Nominal capacity	Nominal voltage	Upper/Lower cut off voltage
LiNMC	1.3 Ah@0.2C	3.6 V	4.2/2.5 V

$$U_{term,k} = V_{oc,k}(SOC) - U_{p,k} - R_0 I_k + \nu_k \tag{4}$$

where U_{term} is the battery terminal voltage, I is the loading current, V_{oc} is the battery OCV which is a time varying dc voltage source related to SOC, and R_0 is the internal ohmic resistance. Battery dynamic characteristics caused by the diffusion effect and a double layer charging/discharging effects are illustrated by the RC network. R_p is the polarization resistance, C_p is the polarization capacitor, and U_p is the voltage cross C_p. ω_1, ω_2 and ν represent the uncertainties caused by the model and external noise or disturbance, which are uncorrelated zero-mean Gaussian white noise. Δt is the sampling interval and the subscript k represents the time step. With the equivalent circuit model, SOC and U_p are considered as states to be estimated by observers. To simply the model, it is assumed that the model parameters are independent of SOC. However, the dependence of model parameters on temperatures is well studied.

- Parameter identification with RLS

The RLS is applied to identify the model parameters including R_0, R_p, and C_p, and the linear identifiable form (5)

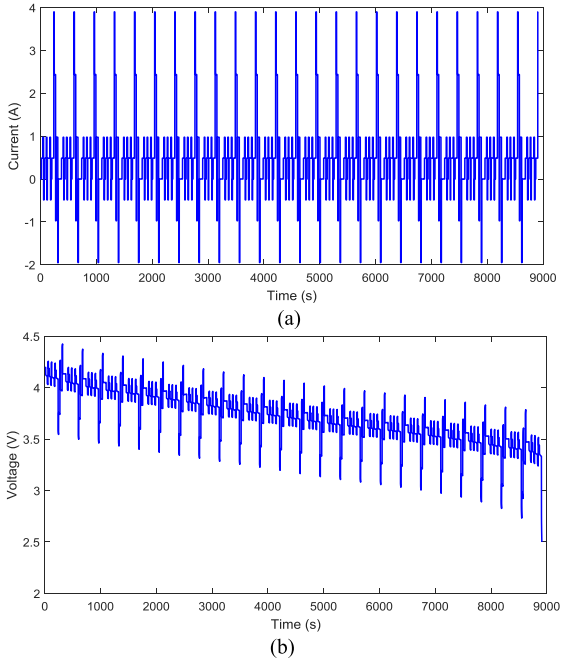

FIGURE 4. DST test profile: (a) current; (b) voltage.

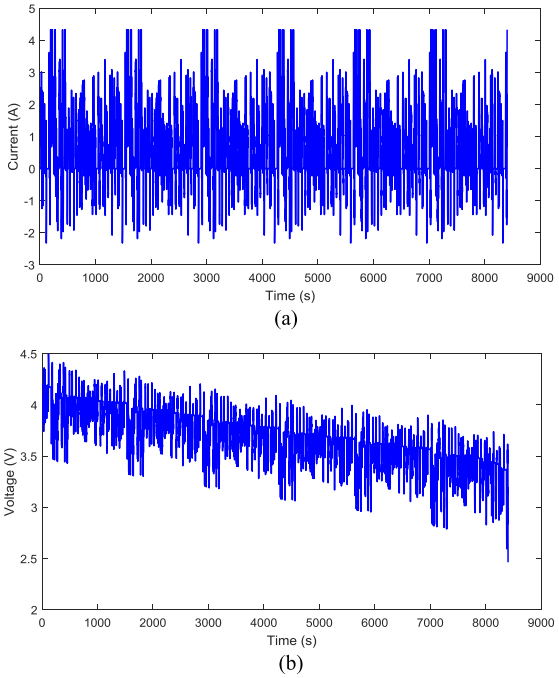

FIGURE 5. FUDS test profile: (a) current; (b) voltage.

is obtained by iteratively substituting (3) into (4):

$$\Delta U_{k+1} = a \cdot \Delta U_k + b \cdot I_k + c \cdot I_{k+1} \tag{5}$$

where $\Delta U_k = V_{oc,k}(SOC) - U_{term,k}$, $a = \exp\left(-\frac{\Delta t_k}{R_p C_p}\right)$, $b = R_p - R_p \cdot \exp\left(-\frac{\Delta t_k}{R_p C_p}\right) - R_0 \cdot \exp\left(-\frac{\Delta t_k}{R_p C_p}\right)$, and $c = R_0$. Assume $\Delta t_k = \Delta t$ for $k = 1, 2, \ldots, N$, then a, b, and c are constants and linear least square (LLS) is applicable for the identification of coefficients in (5) thereby the values of R_0, R_p, and C_p.

- Parameter identification with MPSO

The determination of the parameters R_0, R_p, and C_p can be formulated as an optimization problem (6) to minimize the mean squared error (MSE) between observed ΔU_{k+1} and values of $\Delta \hat{U}_{k+1}$ calculated by (4) - (5):

$$\min MSE = \frac{1}{N-1} \sum_{i=1}^{N-1} \left(\Delta \hat{U}_{k+1} - \Delta U_{k+1}\right)^2 \tag{6}$$

In this paper, the solution of (6) is obtained by using the MPSO algorithm [38]. This method required $U_{p,1}$, and if its value is unknown it can be considered as an unknow parameter to be determined together with R_0, R_p, and C_p. The advantages of the proposed method over RLS will be illustrated with experimental data.

2) COMBINED MODEL

The combined model in (7) is also used to describe the dynamic characteristics of the battery. This model linearly depends on parameters k_0, k_1, k_2, k_3, k_4, and R_0, hence the

TABLE 2. Identified parameters by two algorithms under DST test profile at room temperature.

Parameter	$R_0(\Omega)$	$R_p(\Omega)$	C_p(F)
LS	0.1477	0.0597	728.5
MPSO	0.1556	0.0497	2717.1

TABLE 3. Modeling errors by two different algorithms.

Profile	LS		MPSO	
	MAE (V)	RMSE (V)	MAE (V)	RMSE (V)
DST	0.0117	0.0184	0.0084	0.0150
FUDS	0.0132	0.0238	0.0128	0.0219

LLS is applied to derive these parameters.

$$U_{term,k} = k_0 - \frac{k_1}{SOC_k} - k_2 SOC_k + k_3 \ln(SOC_k) + k_4 (1 - SOC_k) - R_0 I_k \tag{7}$$

C. EXPERIMENTS

The battery test bench consists of a Votsch thermal chamber, an Arbin battery test system BT2000, and a host computer with Arbin's Mits Pro Software shown in Fig. 2. This test bench was also used in [6] and [7]. The cylindrical B18650CD battery (LiNMC) manufactured by BAK (Shenzhen, P. R. China) is used in the test, and the key specifications are shown in Table 1.

1) OCV-SOC TEST

To obtain the relationship between SOC and OCV at various temperatures, the OCV-SOC test is conducted at temperatures

TABLE 4. Fitted parameters and modeling errors at different temperatures.

Temperature (^{0}C)	$R_0(\Omega)$	$R_p(\Omega)$	C_p(F)	MAE (V)		RMSE (V)	
				DST	FUDS	DST	FUDS
0	0.1953	0.0731	508.5	0.0138	0.0194	0.0230	0.0281
10	0.1855	0.0842	1163.3	0.0153	0.0199	0.0252	0.0283
20	0.1742	0.0579	1804.3	0.0112	0.0227	0.0197	0.0438
30	0.1699	0.0432	3251.0	0.0082	0.0109	0.0141	0.0180
40	0.1649	0.0361	2821.5	0.0079	0.0069	0.0120	0.0100
50	0.1603	0.0157	2405.8	0.0069	0.0064	0.0124	0.0081

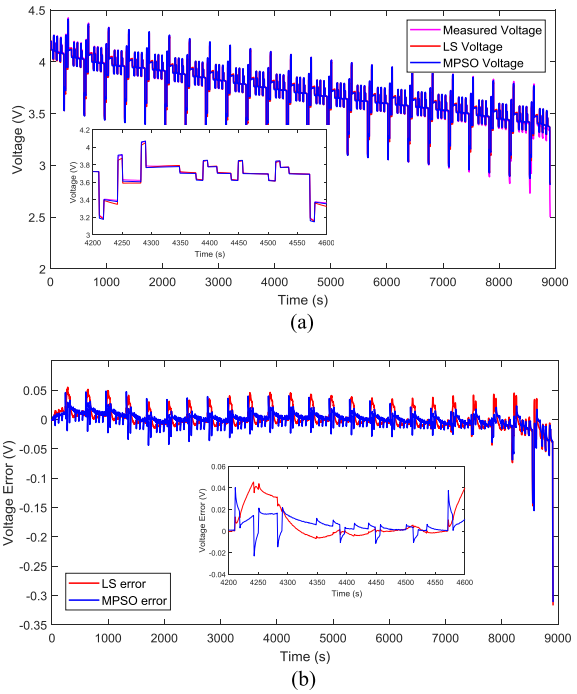

FIGURE 6. Modeling performance by the two algorithms: (a) modeling voltage; (b) modeling error.

from 0 °C to 50 °C at an interval of 10 °C as well as at room temperature 25 °C. The test procedures are described in detail in [6]. The OCV-SOC curves are depicted in Fig. 3. It is observable in Fig. 3(a) that the charging and discharging curves show hysteresis phenomenon. To mitigate the effects of hysteresis and internal ohmic resistance, the averaged cell voltage is used to compute the OCV. The OCV-SOC curves at three different temperatures in Fig. 3(b) show that the OCV difference caused by temperature is not very significant for LiNMC lithium-ion battery especially when the SOC is greater than 10%. Two approaches are adopted to describe the OCV-SOC relationship, OCV-SOC table and seventh polynomial function. The former is used by the UKF algorithm while the latter is employed by the EKF algorithm for SOC estimation in this study.

2) MODEL IDENTIFICATION AND VALIDATION TESTS

Famous test profiles including the dynamic stress test (DST) and the federal urban driving schedule (FUDS) are executed on the battery cells at temperatures from 0 °C to 50 °C at an interval of 10 °C and room temperature. The current profiles and the corresponding terminal voltage at room temperature are depicted in Fig. 4 and Fig. 5, respectively. The DST tests are utilized to identify the battery model parameters, while the FUDS tests are used to evaluate the accuracy of the model as well as the correctness of SOC estimation.

TABLE 5. Fitted parameters of combined model at different temperatures.

Temperature (^{0}C)	k_0	k_0	k_0	k_0	k_0	R_0 (Ω)
RT	3.1867	0.0241	-0.9656	-0.1787	-0.0083	0.1567
0	3.0507	0.1063	-1.1480	-0.4206	-0.0089	0.2061
10	3.0359	0.074	-1.1587	-0.3710	-0.0072	0.1885
20	3.1139	0.0397	-1.0604	-0.2524	-0.0062	0.1761
30	3.1786	0.0231	-0.9798	-0.1789	-0.0078	0.1709
40	3.1585	0.0230	-1.0125	-0.1908	-0.0051	0.1715
50	3.6544	0.0000	-0.3960	0.11950	-0.0240	0.1619

RT: room temperature

D. MODEL CALIBRATION

1) EQUIVALENT CIRCUIT MODEL

The performance in parameter identification by the two algorithms, RLS and MPSO, are compared. The identified parameters based on the DST test profile at room temperature are summarized in Table 2 while the measured and modeling voltages as well as the modeling errors by the two algorithms are depicted in Fig. 6.

The values of internal resistance R_0 obtained by two algorithms are very close, and the main difference lies in the values of the first-order RC network which describes the dynamic behavior of the battery. The time constant ($\tau = R_pC_p$) of the RC network derived by the MPSO algorithm is much longer than that by the RLS algorithm. It usually takes several hours to get the battery totally relaxed, thus the MPSO algorithm better describes the battery behavior which can be demonstrated by the voltage errors in Fig. 6(b).

The mean absolute error (MAE) and the root mean squared error (RMSE) are employed together to evaluate the goodness-of-fit of the model. In Table 3, the modeling errors by the two algorithms are compared where the DST and FUDS are used as the training and test data set, respectively. The MPSO algorithm greatly improves the model accuracy in terms of MAE and RMSE on the DST profiles. The MPSO also performs better on the FUDS profiles as expected. Thus, the MPSO algorithm is chosen as the algorithm to identify the parameters at different temperature, and the identified parameters and modeling errors are summarized in Table 4.

TABLE 6. Comparison of modeling errors of different battery models.

Temperature (^{0}C)	MAE (V)				RMSE (V)			
	DST		FUDS		DST		FUDS	
	CM	ECM	CM	ECM	CM	ECM	CM	ECM
RT	0.0085	0.0084	0.0111	0.0128	0.0146	0.0150	0.0171	0.0219
0	0.0197	0.0138	0.0381	0.0194	0.0300	0.0230	0.0520	0.0281
10	0.0144	0.0153	0.0242	0.0199	0.0242	0.0252	0.0331	0.0283
20	0.0107	0.0112	0.0189	0.0227	0.0189	0.0197	0.0303	0.0438
30	0.0082	0.0082	0.0104	0.0109	0.0136	0.0141	0.0151	0.0180
40	0.0070	0.0079	0.0086	0.0069	0.0100	0.0120	0.0112	0.0100
50	0.0242	0.0069	0.0226	0.0064	0.0319	0.0124	0.0301	0.0081

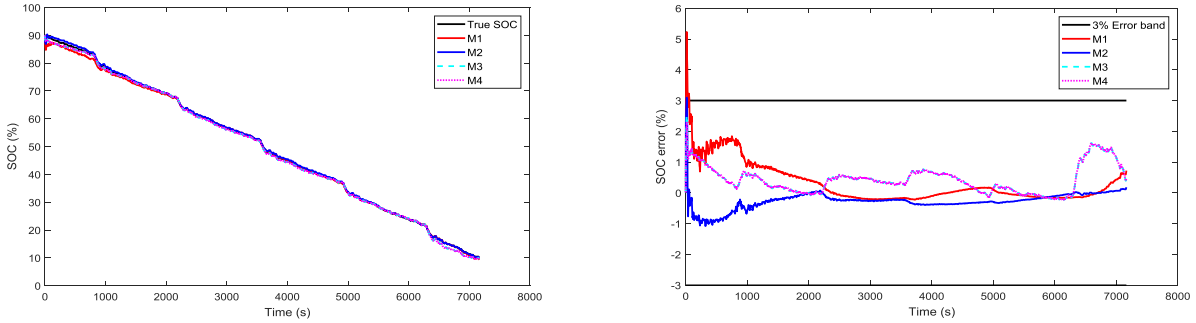

FIGURE 7. SOC estimation with an initial SOC of 90%: (a) SOC estimation; (b) SOC estimation error.

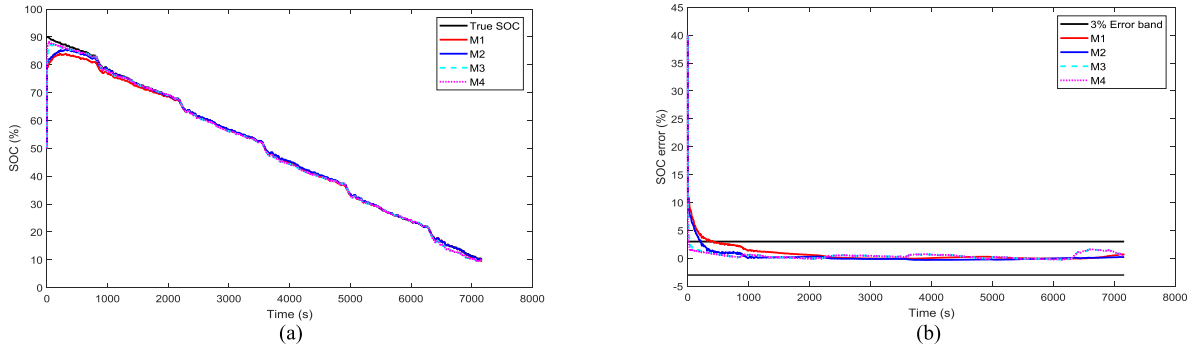

FIGURE 8. SOC estimation with an initial SOC of 50%: (a) SOC estimation; (b) SOC estimation error.

TABLE 7. Nomination of methods used for SOC estimation.

	EKF	UKF
equivalent circuit model (ECM)	M1	M2
combined model (CM)	M3	M4

2) COMBINED MODEL

The parameters at different temperatures are listed in Table 5 while the comparison of the errors by this model against equivalent circuit model is shown in Table 6. From Table 6, it is observable that no model dominates the other for all the temperatures in terms of MAE and RMSE.

III. SOC ESTIMATION AND ANALYSIS

To estimate the state of a dynamic linear system, Kalman filter (KF) is an optimal recursive solution, which has been widely used in various fields such as navigation, target tracking, and global positioning. Since KF is only available for linear system, two extensions of KF including EKF and UKF are applied into lithium-ion battery SOC estimation. The basic idea of KF is to compare the measured terminal voltage with the modeling terminal voltage, and the difference is fed back to correct the predicted SOC by a gain matrix. EKF and UKF are developed to deal with the nonlinear problems. A linearization is realized at each step to approximate the nonlinear system by the EKF algorithm. The UKF algorithm addresses the approximation problems of EKF by introducing the concept of weighted sigma points, which are deterministically selected from the Gaussian approximation. These points propagate through the true nonlinearity, and the mean and covariance of the Gaussian approximation are then re-estimated. The details on the EKF and UKF algorithms and their applications in SOC estimation are well described in [6] and [7].

The FUDS tests are employed to evaluate the performance of SOC estimation. The SOC ranging from 90% to 10% is

TABLE 8. Comparison of SOC estimation with different initial SOCs.

Initial SOC (%)	RMSE (%)				Convergence Rate (s)			
	M1	M2	M3	M4	M1	M2	M3	M4
90	0.7229	0.395	0.6233	0.6193	58	18	1	1
80	0.9732	0.4755	0.6627	0.6399	126	34	17	2
70	1.1884	0.7683	0.7429	0.6787	213	106	23	4
60	1.2962	0.9644	0.8509	0.7360	247	152	27	7
50	1.6229	1.2076	0.9790	0.8070	424	217	29	16
40	1.6080	1.5764	1.1221	0.8885	361	349	34	17
30	1.7390	1.5995	1.2772	0.9789	421	311	37	18
20	2.8722	1.6880	1.4438	1.0879	918	310	49	20
10	6.7206	2.3951	2.0065	1.7780	1783	567	129	104

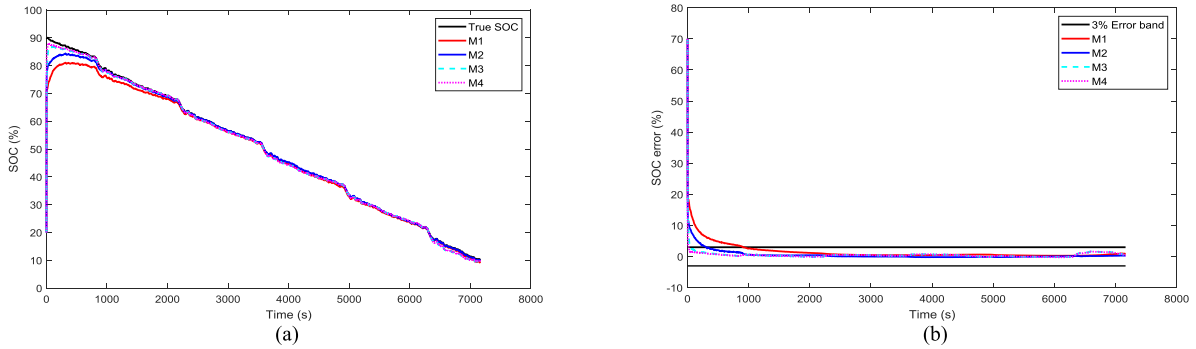

FIGURE 9. SOC estimation with an initial SOC of 20%: (a) SOC estimation; (b) SOC estimation error.

TABLE 9. Robustness evaluation of soc estimation against current noise.

	Initial SOC (%)	M1	M1*	M2	M2*	M3	M3*	M4	M4*
RMSE	90%	0.7229	0.3428	0.3950	0.6700	0.6233	1.2562	0.6193	0.6237
	50%	1.6229	2.1235	1.2076	1.7661	0.9790	0.8989	0.8070	0.7957
	20%	2.8722	3.1969	1.6880	1.7369	1.4438	1.3396	1.0879	1.0578
Conv. Rate (s)	90%	58	2	18	2	1	286	1	29
	50%	424	920	217	468	29	11	16	26
	20%	918	1117	310	405	49	17	20	28

M*: method M applied to estimate SOC with the noisy current.

considered as the parameters vary slightly within the range and the battery SOC is seldom permitted to exceed this range in battery management systems for EVs. The performance of SOC estimation methods handling various practical problems including unknown initial SOC, current noise, and temperature effects is studied. To clearly distinct the observers and models used in each SOC estimation method, the nomination of different methods is given in Table 7.

A. SOC ESTIMATION WITH UNKNOWN INITIAL VALUE AT ROOM TEMPERATURE

To illustrate the robustness of EKF and UKF against unknown initial SOC, the behavior including estimation accuracy and convergence rate of EKF and UKF in SOC estimation with unknown initial SOCs is discussed. The accuracy is illustrated by RMSE, and the convergence rate is defined as the time that the estimated SOC converges to the $\pm 3\%$ error bands.

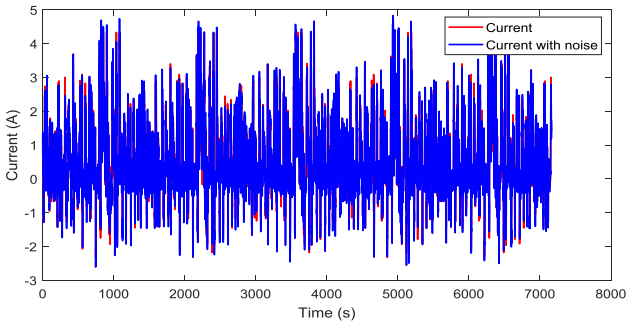

FIGURE 10. Comparison between the measured current and noisy current.

The estimation accuracy and convergence rate by EKF and UKF with different settings of initial SOCs from 90% to 10% at the step interval of 10% is summarized in Table 8. It is observable that the RMSE and convergence rate generally increases with increasing initial SOC errors. The UKF

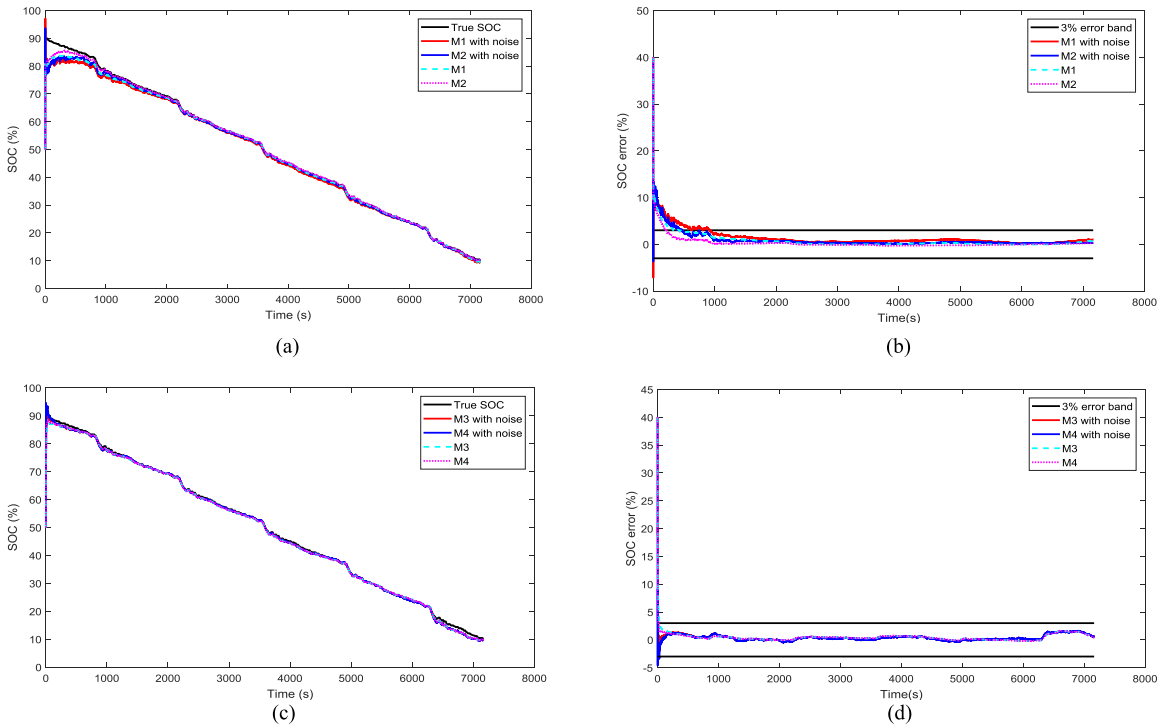

FIGURE 11. Illustration of SOC estimation with and without current noise: (a) SOC estimation with circuit equivalent; (b) SOC estimation error with circuit equivalent model; (c) SOC estimation with combined model; (d) SOC estimation error with combined model.

algorithm based on combined model (M4) generally provides most accurate estimation, while the EKF algorithm based on equivalent circuit model (M1) performs worst. The UKF converges much faster than EKF regardless of the lithium-ion battery model used. The advantage of UKF over EKF with combined model is not as significant as with equivalent circuit model. This can be partially explained that with equivalent circuit model the UKF employs OCV-SOC table which is more accurate than the polynomial OCV-SOC relationship used by EKF.

The estimation of SOC by different methods with initial SOC settings of 90%, 50%, and 20% are illustrated in Figs. 7-9. In Fig. 7, the initial setting of SOC is set to the true value, however, the EKF and UKF based on the equivalent circuit model take some time to converge to the true SOC. This is partially due to that the EKF and UKF based on the equivalent circuit model should also accurately estimate U_p. From these figures, it's clear that the convergence of the estimation of SOC based on combined model is much faster than that based on the equivalent circuit model. This leads to the higher accuracy of combined model based estimation of SOC. However, the combined model based estimation of SOC is less reliable at low true SOCs due to large errors.

B. SOC ESTIMATION WITH CURRENT NOISE AT ROOM TEMPERATURE

To illustrate the robustness of EKF and UKF against current noise due to sensor drift in SOC estimation, a zero-mean Gaussian noise whose variance equals 0.25 A^2 is added into the measured current. The comparison between the measured current and the noisy current is depicted in Fig. 10. The amplitude of the noise can be as high as 0.5 A which takes up 12% of the maximal current value under FUDS test.

The performance of SOC estimation by different methods is given in Table 9. As the noise is randomly added into the current, the impacts of current noise on SOC estimation is also random that the performance can be improved or degraded in terms of estimation accuracy and convergence rate. From Fig. 11, however, it is observable that both the EKF and UKF can handle current noise for SOC estimation regardless of the lithium-ion battery model used.

TABLE 10. Battery discharge capacity (Ah) under different loads at various temperatures.

Profile	0 ^{0}C	10 ^{0}C	20 ^{0}C	30 ^{0}C	40 ^{0}C	50 ^{0}C	RT
C/25	1.3203	1.3508	1.3602	1.3655	1.3658	1.3605	1.3659
1C	1.0842	1.1799	1.2605	1.3172	1.3446	1.3563	1.2986
DST	0.9631	1.1116	1.2176	1.2717	1.3145	1.3622	1.2732
FUDS	0.9146	1.0781	1.2750	1.2881	1.2922	1.3090	1.2864

C. SOC ESTIMATION AT VARIOUS TEMPERATURES

The OCV-SOC relationship and model parameters depend on temperature. Moreover, the battery discharging capacity under different loading profiles are related with temperatures

TABLE 11. RMSE (%) of SOC estimation by different methods.

Initial SOC	Temp. (^{0}C)	M1		M2		M3		M4	
		No Update	Update	No Update	Update	No Update	Update	No Update	Update
90%	0	9.087	3.6672	8.7711	3.3501	9.163	0.6163	9.1792	0.6251
	10	5.6014	1.266	5.3142	0.7691	5.529	0.4595	5.5219	0.4553
	20	2.9307	0.9876	2.3733	0.4691	2.9614	0.7114	2.9582	0.7077
	30	1.6143	0.5802	0.8725	0.2283	1.3138	0.6032	1.3103	0.6015
	40	0.9109	0.6745	0.4242	0.2881	0.5887	0.5598	0.585	0.5563
	50	1.057	0.9033	1.1004	0.5281	0.744	2.6411	0.7427	2.6399
50%	0	9.1431	3.7208	8.8100	3.4477	9.2612	0.9651	9.2090	0.8364
	10	5.6762	1.3980	5.4628	1.1454	5.6141	0.8990	5.5623	0.7049
	20	3.0308	1.1404	2.6845	0.7481	3.0727	1.0309	3.0094	0.8751
	30	1.7605	0.8027	1.2491	0.5428	1.5296	0.9292	1.4138	0.7797
	40	1.0979	0.8760	0.7329	0.5883	0.9465	0.9252	0.7783	0.7543
	50	1.1751	1.0346	1.2318	0.7241	1.0384	2.7247	0.8989	2.6833
20%	0	9.2427	3.8276	8.9261	3.6666	9.3882	1.8699	9.2608	1.6018
	10	5.8047	1.6755	5.7050	1.7035	5.7525	1.5235	5.6235	1.2051
	20	3.2154	1.4269	3.2042	1.4308	3.2648	1.4809	3.1006	1.1605
	30	2.0115	1.1416	2.0186	1.0030	1.8727	1.3848	1.5944	1.0557
	40	1.3888	1.1743	1.4065	1.0748	1.4134	1.3912	1.0640	1.0355
	50	1.3926	1.2586	1.4607	1.0728	1.4731	2.9467	1.1548	2.8047

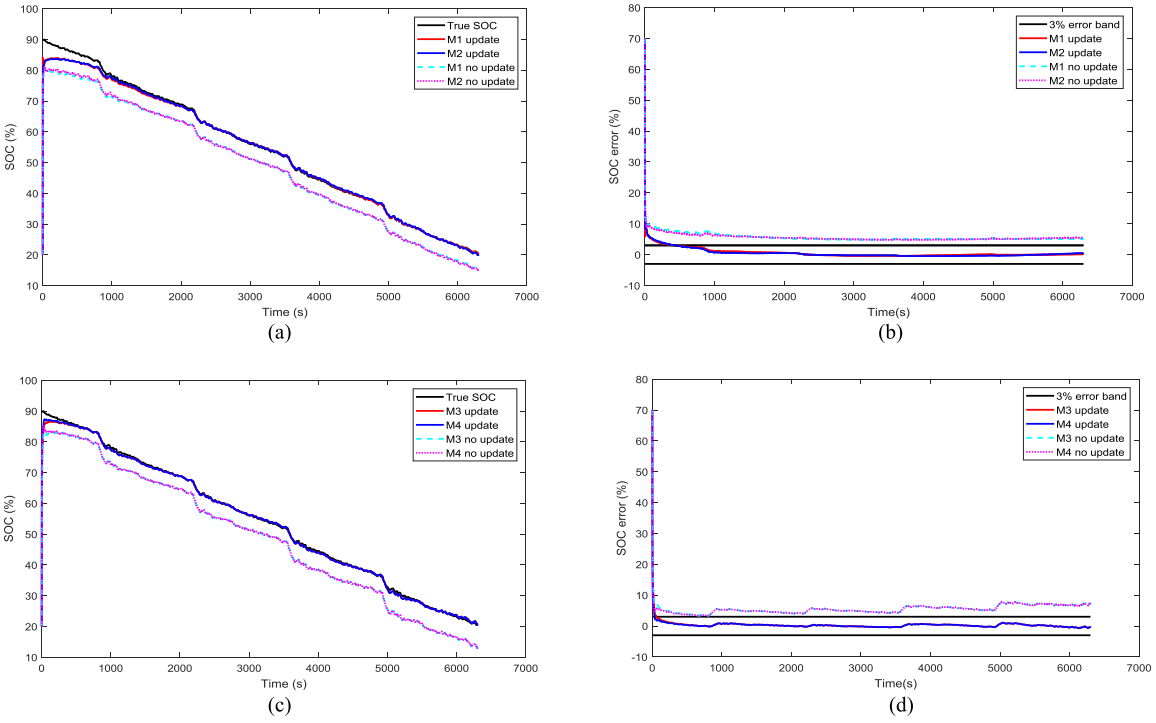

FIGURE 12. SOC estimation with and without updates of parameters at 10 °C: (a) SOC estimation with circuit equivalent; (b) SOC estimation error with circuit equivalent model; (c) SOC estimation with combined model; (d) SOC estimation error with combined model.

as shown in Table 10. At infinitesimal discharging rate (C/25), the discharging capacity varies less than 4% of the nominal capacity for various temperatures. However, the situation is very different for DST and FUDS test profiles in which the variation can reach 30% of the nominal capacity. At low temperature (0 °C) the discharge capacity under DST and FUDS is much smaller than that at high temperature (50 °C). This is explained by the battery performance degradation due to the reducing internal chemical reaction at low temperature, and that's why reheating is required for a battery to crank at low temperature. In this paper, the robustness of EKF and UKF based on different lithium-ion battery model against temperature for SOC estimation is also investigated.

The accuracy of SOC estimation at different temperatures with and without updates of parameters are summarized in Table 11. *No update* means that the parameters at room temperature are employed to estimate SOC at other temperatures. It's observable that the updates of parameters can greatly improve EKF and UKF based SOC estimation accuracy with equivalent circuit model at any temperature regardless of the settings of initial SOC. However, at 0 °C the estimation based on equivalent circuit model is much

less accurate than at other temperatures. With the combined model, the updates of parameters improve the estimation accuracy at all the temperatures except at 50 °C due to the inaccurate model. The UKF generally outperformed EKF with a given model, but no method dominates the others at all the temperatures considering the battery model utilized. Fig. 12 depicts the SOC estimation with and without updates of parameters at 10 °C. It is observable that the updates of parameters greatly reduce the estimation errors for both UKF and EKF.

IV. CONCLUSION

In this paper, the robustness of EKF and UKF for lithium-ion battery SOC estimation against core problems such as unknown initial SOC, current noise, and temperature effects is studied. As EKF and UKF are sensitive to the battery model, two models including first-order RC equivalent circuit model and combined model are utilized to characterize the dynamic behavior of the lithium-ion battery. The methods for model parameter identification is also discussed. With equivalent circuit model, the MPSO outperformed RLS for model parameter identification in terms of modeling accuracy. However, for the considered battery models no one outperformed the other at all the test temperatures.

The experiment data on a commercial lithium-ion battery cell (LiNMC) is utilized to evaluate the performance of different methods in SOC estimation. Computational results illustrate that UKF algorithm generally outperforms EKF algorithm in terms of SOC estimation accuracy and convergence rate with unknow initial SOC. However, the advantages of UKF over EKF are more significant with the equivalent circuit model than with the combined mode. Both UKF algorithm and EKF algorithm show strong robustness against current noise regardless of the battery model. More importantly, it's of great importance to update the parameters at different temperatures for both EKF and UKF to improve the estimation accuracy. It also should be noted that the accuracy of combined model is greatly reduced at high temperature leading to inaccurate SOC estimation with updates of model parameters.

REFERENCES

[1] Q. Wang, B. Jiang, B. Li, and Y. Y. Yan, "A critical review of thermal management models and solutions of lithium-ion batteries for the development of pure electric vehicles," *Renew. Sustain. Energy Rev.*, vol. 64, pp. 106–128, Oct. 2016.

[2] M. A. Hannan, M. S. H. Lipu, A. Hussain, and A. Mohamed, "A review of lithium-ion battery state of charge estimation and management system in electric vehicle applications: Challenges and recommendations," *Renew. Sustain. Energy Rev.*, vol. 78, pp. 834–854, Oct. 2017.

[3] F. C. Sun, R. Xiong, and H. W. He, "A systematic state-of-charge estimation framework for multi-cell battery pack in electric vehicles using bias correction technique," *Appl. Energy*, vol. 162, pp. 1399–1409, Jan. 2016.

[4] C. Zou, X. Hu, Z. Wei, T. Wik, and B. Egardt, "Electrochemical estimation and control for lithium-ion battery health-aware fast charging," *IEEE Trans. Ind. Electron.*, vol. 65, no. 8, pp. 6635–6645, Aug. 2018.

[5] G. Dong, J. Wei, C. Zhang, and Z. Chen, "Online state of charge estimation and open circuit voltage hysteresis modeling of $LiFePO_4$ battery using invariant imbedding method," *Appl. Energy*, vol. 162, pp. 163–171, Jan. 2016.

[6] Y. Xing, W. He, M. Pecht, and K. L. Tsui, "State of charge estimation of lithium-ion batteries using the open-circuit voltage at various ambient temperatures," *Appl. Energy*, vol. 113, pp. 106–115, Jan. 2014.

[7] F. Yang, Y. Xing, D. Wang, and K.-L. Tsui, "A comparative study of three model-based algorithms for estimating state-of-charge of lithium-ion batteries under a new combined dynamic loading profile," *Appl. Energy*, vol. 164, pp. 387–399, Feb. 2016.

[8] J. H. Aylor, A. Thieme, and B. W. Johnso, "A battery state-of-charge indicator for electric wheelchairs," *IEEE Trans. Ind. Electron.*, vol. 39, no. 5, pp. 398–409, Oct. 1992.

[9] J. C. A. Antón, P. J. G. Nieto, C. B. Viejo, and J. A. V. Vilán, "Support vector machines used to estimate the battery state of charge," *IEEE Trans. Power Electron.*, vol. 28, no. 12, pp. 5919–5926, Dec. 2013.

[10] B. Xiong, J. Zhao, Y. Su, Z. Wei, and M. Skyllas-Kazacos, "State of charge estimation of vanadium redox flow battery based on sliding mode observer and dynamic model including capacity fading factor," *IEEE Trans. Sustain. Energy*, vol. 8, no. 4, pp. 1658–1667, Oct. 2017.

[11] B. Xia, C. Chen, Y. Tian, W. Sun, Z. Xu, and W. Zheng, "A novel method for state of charge estimation of lithium-ion batteries using a nonlinear observer," *J. Power Sources*, vol. 270, pp. 359–366, Dec. 2014.

[12] K. S. Ng, C.-S. Moo, Y.-P. Chen, and Y.-C. Hsieh, "Enhanced coulomb counting method for estimating state-of-charge and state-of-health of lithium-ion batteries," *Appl. Energy*, vol. 86, no. 9, pp. 1506–1511, Sep. 2009.

[13] K.-S. Ng, C.-S. Moo, Y.-P. Chen, and Y.-C. Hsieh, "State-of-charge estimation for lead-acid batteries based on dynamic open-circuit voltage," in *Proc. IEEE 2nd Int. Power Energy Conf. (PECon)*, Dec. 2008, pp. 972–976.

[14] H. Chaoui, C. C. Ibe-Ekeocha, and H. Gualous, "Aging prediction and state of charge estimation of a $LiFePO_4$ battery using input time-delayed neural networks," *Elect. Power Syst. Res.*, vol. 146, pp. 189–197, May 2017.

[15] P. Singh, R. Vinjamuri, X. Wang, and D. Reisner, "Design and implementation of a fuzzy logic-based state-of-charge meter for Li-ion batteries used in portable defibrillators," *J. Power Sources*, vol. 162, no. 2, pp. 829–836, 2006.

[16] I. H. Li, W. Y. Wang, S. F. Su, and Y. S. Lee, "A merged fuzzy neural network and its applications in battery state-of-charge estimation," *IEEE Trans. Energy Convers.*, vol. 22, no. 3, pp. 697–708, Sep. 2007.

[17] X. Hu, S. E. Li, and Y. Yang, "Advanced machine learning approach for lithium-ion battery state estimation in electric vehicles," *IEEE Trans. Transport. Electrific.*, vol. 2, no. 2, pp. 140–149, Jun. 2016.

[18] G. O. Sahinoglu, M. Pajovic, Z. Sahinoglu, Y. Wang, P. Orlik, and T. Wada, "Battery state-of-charge estimation based on regular/recurrent Gaussian process regression," *IEEE Trans. Ind. Electron.*, vol. 65, no. 5, pp. 4311–4321, May 2018.

[19] C. Zou, X. Hu, Z. Wei, and X. Tang, "Electrothermal dynamics-conscious lithium-ion battery cell-level charging management via state-monitored predictive control," *Energy*, vol. 141, pp. 250–259, Dec. 2017.

[20] C. Zou, X. Hu, S. Dey, L. Zhang, and X. Tang, "Nonlinear fractional-order estimator with guaranteed robustness and stability for lithium-ion batteries," *IEEE Trans. Ind. Electron.*, vol. 65, no. 7, pp. 5951–5961, Jul. 2018.

[21] C. Zhang, W. Allafi, Q. Dinh, P. Ascencio, and J. Marco, "Online estimation of battery equivalent circuit model parameters and state of charge using decoupled least squares technique," *Energy*, vol. 142, pp. 678–688, Jan. 2018.

[22] P. Malysz, J. Ye, R. Gu, H. Yang, and A. Emadi, "Battery state-of-power peak current calculation and verification using an asymmetric parameter equivalent circuit model," *IEEE Trans. Veh. Technol.*, vol. 65, no. 6, pp. 4512–4522, Jun. 2016.

[23] J. H. Meng, G. Z. Luo, and F. Gao, "Lithium polymer battery state-of-charge estimation based on adaptive unscented Kalman filter and support vector machine," *IEEE Trans. Power Electron.*, vol. 31, no. 3, pp. 2226–2238, Mar. 2016.

[24] X. Chen, W. Shen, M. Dai, Z. Cao, J. Jin, and A. Kapoor, "Robust adaptive sliding-mode observer using RBF neural network for lithium-ion battery state of charge estimation in electric vehicles," *IEEE Trans. Veh. Technol.*, vol. 65, no. 4, pp. 1936–1947, Apr. 2016.

[25] H. Pan, Z. Lü, W. Lin, J. Li, and L. Chen, "State of charge estimation of lithium-ion batteries using a grey extended Kalman filter and a novel open-circuit voltage model," *Energy*, vol. 138, pp. 764–775, Nov. 2017.

[26] G. Dong, J. Wei, and Z. Chen, "Kalman filter for onboard state of charge estimation and peak power capability analysis of lithium-ion batteries," *J. Power Sources*, vol. 328, pp. 615–626, Oct. 2016.

[27] Q. Zhu, X. Hu, N. Xiong, and G.-D. Hu, "H_∞-based nonlinear observer design for state of charge estimation of lithium-ion battery with polynomial parameters," *IEEE Trans. Veh. Technol.*, vol. 66, no. 12, pp. 10853–10865, Dec. 2017.
[28] C.-Z. Liu *et al.*, "A state of charge estimation method based on H_∞ observer for switched systems of lithium-ion nickel–manganese–cobalt batteries," *IEEE Trans. Ind. Electron.*, vol. 64, no. 10, pp. 8128–8137, Oct. 2017.
[29] B. J. Wang, Z. Liu, S. Li, S. Moura, and H. Peng, "State-of-charge estimation for lithium-ion batteries based on a nonlinear fractional model," *IEEE Trans. Control Syst. Technol.*, vol. 25, no. 1, pp. 3–11, Jan. 2017.
[30] X. Hu, F. Sun, and Y. Zou, "Estimation of state of charge of a lithium-ion battery pack for electric vehicles using an adaptive Luenberger observer," *Energies*, vol. 4, no. 9, pp. 1586–1603, 2011.
[31] G. L. Plett, "Extended Kalman filtering for battery management systems of LiPB-based HEV battery packs: Part 3. State and parameter estimation," *J. Power Sources*, vol. 134, no. 2, pp. 277–292, 2004.
[32] G. L. Plett, "Sigma-point Kalman filtering for battery management systems of LiPB-based HEV battery packs: Part 2: Simultaneous state and parameter estimation," *J. Power Sources*, vol. 161, no. 2, pp. 1369–1384, 2006.
[33] S. Sepasi, R. Ghorbani, and B. Y. Liaw, "A novel on-board state-of-charge estimation method for aged Li-ion batteries based on model adaptive extended Kalman filter," *J. Power Sources*, vol. 245, pp. 337–344, Jan. 2014.
[34] S. Peng, C. Chen, H. Shi, and Z. Yao, "State of charge estimation of battery energy storage systems based on adaptive unscented Kalman filter with a noise statistics estimator," *IEEE Access*, vol. 5, pp. 13202–13212, 2017.
[35] H. Aung, K. S. Low, and S. T. Goh, "State-of-charge estimation of lithium-ion battery using square root spherical unscented Kalman filter (Sqrt-UKFST) in nanosatellite," *IEEE Trans. Power Electron.*, vol. 30, no. 9, pp. 4774–4783, Sep. 2015.
[36] Y. Zou, X. Hu, H. Ma, and S. E. Li, "Combined state of charge and state of health estimation over lithium-ion battery cell cycle lifespan for electric vehicles," *J. Power Sources*, vol. 273, pp. 793–803, Jan. 2015.
[37] C. Zou, C. Manzie, D. Nešić, and A. G. Kallapur, "Multi-time-scale observer design for state-of-charge and state-of-health of a lithium-ion battery," *J. Power Sources*, vol. 335, pp. 121–130, Dec. 2016.
[38] X. Hu, S. Li, and H. Peng, "A comparative study of equivalent circuit models for Li-ion batteries," *J. Power Sources*, vol. 198, pp. 359–367, Jan. 2012.
[39] G. Bai, P. Wang, C. Hu, and M. Pecht, "A generic model-free approach for lithium-ion battery health management," *Appl. Energy*, vol. 135, pp. 247–260, Dec. 2014.
[40] Z. Wei, K. Tseng, N. Wai, T. Lim, and M. Skyllas-Kazacos, "Adaptive estimation of state of charge and capacity with online identified battery model for vanadium redox flow battery," *J. Power Sources*, vol. 332, pp. 389–398, Nov. 2016.

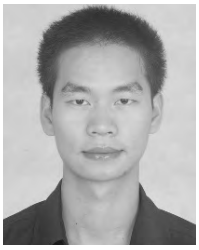

CHAO HUANG (S'16–M'17) received the B.Eng. degree in electrical engineering and automation from the Harbin Institute of Technology, China, in 2011, the M.S. degree in intelligent transport system from the University of Technology of Compiègne, France, in 2013, and the Ph.D. degree in systems engineering and engineering management from the City University of Hong Kong, Hong Kong, in 2017.

He was appointed as a Post-Doctoral Fellow with the Department of Systems Engineering and Engineering Management, City University of Hong Kong. He is currently a Lecturer with the School of Automation, Guangdong University of Technology. His research interests include photovoltaics, lithium-ion battery, machine learning, and computational intelligence.

ZHENHUA WANG received the Ph.D. degree in engineering from China Agricultural University, China, in 2014. He conducted the Postdoctoral research in soil hydrology with Pennsylvania State University, Pennsylvania, USA, in 2016. He became a Ph.D. Supervisor of agricultural soil and water engineering in 2015.

He is currently the Deputy Dean of the College of Water Conservancy and Architectural Engineering, Shihezi University, and also the Deputy Director of the Key Laboratory of Modern Water-Saving Irrigation Corps. His research interests include the theory and technology of water-saving irrigation in arid area, and the theory and technology of drip irrigation water and salt control.

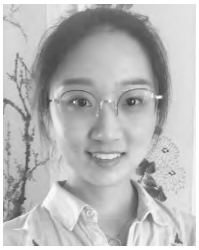

ZIHAN ZHAO is currently pursuing the bachelor's degree in surveying and mapping engineering with the School of Geosciences and Surveying Engineering, China University of Mining and Technology, Beijing, China.

LONG WANG (S'16–M'17) received the M.Sc. degree (Hons.) in computer science from University College London, London, U.K., in 2014, and the Ph.D. degree in systems engineering and engineering management from the City University of Hong Kong, Hong Kong, in 2017.

He is currently an Associate Professor with the Department of Computer Science and Technology, University of Science and Technology Beijing, Beijing, China. His research interests include machine learning, computational intelligence, and computer vision. He was an awardee of the Hong Kong Ph.D. Fellowship in 2014. He serves as an Associate Editor for the IEEE Access.

CHUN SING LAI received the B.Eng. degree (Hons.) in electrical and electronic engineering from Brunel University London, U.K., in 2013. He is currently pursuing the D.Phil. degree in engineering science with the University of Oxford, U.K. He is currently a Visiting Research Fellow with the School of Automation, Guangdong University of Technology, China, and also a Research Fellow with the School of Civil Engineering, University of Leeds. He organized the IEEE SMC Workshop on Smart Grid and Smart City in SMC 2017, Canada. His current interests are in data analytics and energy economics for renewable energy and storage systems.

DONG WANG received the Ph.D. degree with the City University of Hong Kong (CityU) in 2015. He was appointed as a Research Associate, a Senior Research Assistant, and a Post-Doctoral Fellow with CityU from 2015 to 2018. He is currently a Research Fellow with CityU. He was a recipient of the Hong Kong Ph.D. Fellowship in 2012.

His research interests include statistical modeling, prognostics and health management, condition monitoring, fault diagnosis, signal processing, data mining, and nondestructive testing. His research works appear in *Mechanical Systems and Signal Processing*, the *Journal of Sound and Vibration*, ASME Transactions on the *Journal of Vibration and Acoustics*, the IEEE TRANSACTIONS ON RELIABILITY, the IEEE TRANSACTIONS ON INSTRUMENTATION AND MEASUREMENT, the *Journal of Power Sources*, and *Measurement Science and Technology*.

Dr. Wang was invited to be a Reviewer for 50 SCI-indexed journals. In recognition to his contributions to Elsevier and IEEE journals, he was awarded Outstanding Reviewer Status 13 times. He was a lead guest editor/guest editor for several SCI-indexed journals and a referee for the FONDECYT, Chile. He is an Associate Editor for the *Journal of Low Frequency Noise Vibration and Active Control* and an Associate Editor for the IEEE ACCESS.